ACS APPLIED MATERIALS & INTERFACES

Research Article

www.acsami.org

# Solution Processable Benzooxadiazole and Benzothiadiazole Based D-A-D Molecules with Chalcogenophene: Field Effect Transistor Study and Structure Property Relationship

Palas Baran Pati,[†] Satyaprasad P. Senanayak,[‡] K. S. Narayan,*[,‡] and Sanjio S. Zade*[,†]

[†]Department of Chemical Sciences, Indian Institute of Science Education and Research, Kolkata, PO: BCKV campus main office, Mohanpur 741252, Nadia, West Bengal, India

[‡]Chemistry and Physics of Materials Unit, Jawaharlal Nehru Centre for Advanced Scientific Research, Bangalore 560064, Karnataka, India

Supporting Information

**ABSTRACT:** We present here the physicochemical characterization of a series of D-A-D type molecules which comprise benzooxadiazole (BDO) and benzothiadiazole (BDT) core symmetrically linked to two aromatic-heterols (furan (F), thiophene (T) and selenophene (Se)) at 4 and 7-positions. The molecular structures of four compounds **2** (T-BDO-T), **3** (Se-BDO-Se), **5** (T-BDT-T), and **6** (Se-BDT-Se) were determined by single-crystal X-ray diffraction. The combination of chalcogen atoms of benzochalcogenadiazole and chalcogenophene in D-A-D molecules has significant impact on their molecular packing in crystal structures. Structural analyses and theoretical calculations showed that all the molecules are nearly planar. Crystal structures of **2**, **3**, **5**, and **6** showed significant short range interactions such as $\pi\cdots\pi$, CH$\cdots\pi$, S$\cdots\pi$, Se$\cdots\pi$, N$\cdots$H, O$\cdots$H, S$\cdots$H, Se$\cdots$H, S$\cdots$O, and Se$\cdots$N interactions, which influence crystal packing and orientation of the capped aromatic-heterol rings with respect to the central BDO or BDT unit. The $\pi$-stacking interactions have been observed via intermolecular overlap of the donor with acceptor units of the adjacent molecules which facilitate the charge transport process. Good thermal stability and solubility in common organic solvents make them good candidate for flexible electronics. Interestingly, the molecules **2**, **3**, and **6** have the propensity to form ordered crystallites when sheared during the drying process in the thin films. Devices based on these solution processable all organic FETs demonstrated hole mobility as high as 0.08 $cm^2 V^{-1} s^{-1}$ and $I_{on}/I_{off}$ ratio of $10^4$.

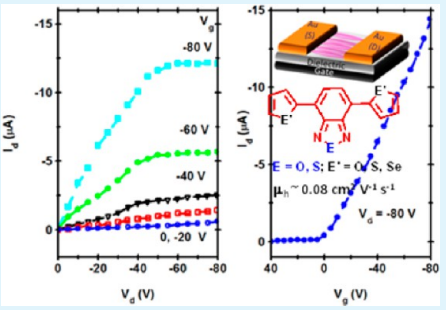


**KEYWORDS:** *donor−acceptor−donor, conjugated small molecules, field effect transistors, benzooxadiazole, benzothiadiazole, structure-property relationship*

## INTRODUCTION

Organic field-effect transistors (OFETs) have recently become more important because of their wide variety of applications in large area electronic circuits such as electronic papers, radio-frequency identification tags, and display devices.[1−5] Cheap manufacturing and potential for printable electronics made them preferable for large-scale low-cost commercial applications. The competitive nature of small molecules relative to polymeric materials can be ascribed to the predominant advantages including well-defined molecular structures, simple synthesis, high purity, easier purification, better batch-to batch reproducibility, and reproducible device performance. The most important one is solubility in common organic solvents which makes small molecules more effective in organic semiconductor devices. This solution processabilty results in easier fabrication by using a more conventional method such as spin coating, printing, and stamping than other relatively expensive processes.[6,7] Charge carrier mobility is a material property determined by the degree of conjugation and the intermolecular arrangement of the organic moieties in the thin films. Molecular packing is a crucial issue in FET devices because $\pi$-stacked structures are considered advantageous since it facilitates charge-carrier mobility due to effective $\pi-\pi$ interactions.[8]

The presence of fused rings with a high degree of planarity and rigidity results in greater crystallinity of molecules. Additionally, extended $\pi$ overlap results in overall improvement in hole or electron mobility. Although, thiophene-based $\pi$-conjugated systems were heavily explored, their selenium counterparts have lately drawn considerable attention as a novel class of $\pi$-conjugated materials exhibiting promising optoelectronic properties. By replacing sulphur with less electronegative and more polarizable selenium (atomistic approach), the band gap, and thus the optical and electronic properties can be tuned.[9−12] Recent discoveries on oligofuran proved the potential of furan-based conjugated systems as promising hole

Received: August 23, 2013
Accepted: November 15, 2013
Published: November 15, 2013

  

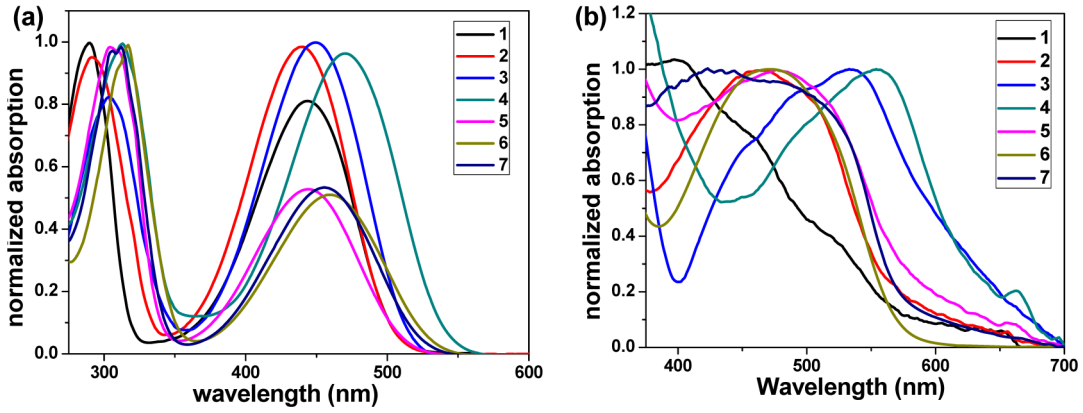


**Figure 1.** (a) Normalized absorption spectra of dilute solution of compounds **1**−**7** in chloroform; (b) normalized absorption spectra of thin film obtained from drop casting method from chloroform solution.

**Table 1. Absorption and Electrochemical Properties of Compounds 1−7**

| | $\lambda_{max}$ (nm) | | | | | | |
|---|---|---|---|---|---|---|---|
| compounds | $CHCl_3$ | thinfilm | $E_{ox}$ (V)[a] | HOMO (eV) | optical band gap (eV) | LUMO (eV) | theoretical HOMO-LUMO gap[b] |
| **1** | 289, 444 | 461 | 1.20 (1.15) | −5.61 | 2.46 | −3.15 | 2.52 |
| **2** | 294, 441 | 462 | 1.34 (1.24) | −5.70 | 2.47 | −3.23 | 2.69 |
| **3** | 305, 450 | 526 | 1.23 (1.16) | −5.62 | 2.41 | −3.21 | 2.73 |
| **4** | 314, 470 | 550 | 0.96 (0.91) | −5.37 | 2.30 | −3.07 | 2.34 |
| **5** | 309, 445 | 485 | 1.23 (1.11) | −5.57 | 2.43 | −3.14 | 2.62 |
| **6** | 317, 461 | 474 | 1.13 (1.05) | −5.51 | 2.33 | −3.18 | 2.68 |
| **7** | 311, 454 | 476 | 1.13 (1.03) | −5.49 | 2.37 | −3.12 | 2.56 |

[a]The values in parentheses correspond to onset oxidation potential of compounds. [b]The values are taken from the most stable conformations.

transporting material.[13] The development of furan-based conjugated systems relies on its enhanced solution processability. Compared to sulfur/selenium-based organic electronic materials, oxygen-based materials are more biodegradable and biocompatible.[14−17]

Among different classes of donor molecules, linear acenes and oligothiophenes are the two most studied classes to date.[18−21] Recent reports of benzo[2,1,3]thiadiazole (BDT) derivatives containing organic moieties showed high electron mobilities and high $I_{on}/I_{off}$ ratios which has been attributed to the strong electron accepting property of BDT and the intermolecular interactions S···N contacts between the thiadiazole rings.[22−24] There are few reports on FET devices using D-A type polymers comprising BDT[25−27] and benzo-[2,1,3]thiadiazole (BDS).[25,28,29] However, the reports on small molecules containing BDT are scarce, and their hole or electron mobility values are reported to be low in OFET devices.[26,30−35] BDT and BDS are very well-established as electron acceptors in D-A conjugated systems whereas their oxygen analogue, benzo[2,1,3]oxadiazole (BDO), has not received sufficient attention.[36−40]

Recently, we have reported the synthesis of furan, thiophene, selenophene, and EDOT-capped BDO molecules and the electrochromic nature of their electrochemically synthesized polymers.[41] Here we report the structures and FET performances of small molecules containing donor−acceptor−donor (D-A-D) architecture where donors are furan, thiophene, selenophene, and EDOT and acceptors are BDO and BDT. To study the structure property relationship between BDO and BDT acceptor moieties (in D-A-D system), we have synthesized BDO-based compounds **1**−**4** and BDT-based compounds **5**−**7**. From the single crystal structure studies, it is clear that D-A-D molecules **2**, **3**, **5**, and **6** are perfectly planar and possess various intra- and intermolecular non-bonding interactions which can facilitate the charge transport. Therefore, these compounds **1**−**7** are studied as active materials in OFET devices. High field effect hole mobility ($\mu_{FET}$) of 0.08 $cm^2\ V^{-1}\ s^{-1}$ and $I_{on}/I_{off} > 10^4$ is obtained from these compounds owing to better $\pi$-stacking, crystalline structure, and molecular planarity.

## RESULTS AND DISCUSSION

**Optical and Electrochemical Properties.** The UV-vis spectra of all monomers were studied in chloroform solutions (Figure 1a) and thin films cast on an ITO coated glass (Figure 1b, Table 1). As shown in Figure 1a, the absorption spectra of **1**−**7** showed two absorption bands; higher energy bands (300-314 nm) due to conjugation and lower energy band (450−470 nm) for charge transfer (CT). The $\lambda_{max}$ values of both peaks shifted to the red region with increase in electron donation capacity of chalcogenophene ring. As EDOT is the significantly electron rich, compound **4** showed the absorption maxima at higher wavelength (317, and 470 nm). Absorption maxima are shifted to the higher wavelength value in the order **1** < **2** < **3** < **4**, where furan, thiophene, selenophene, and EDOT are donor moieties, respectively. The major difference in the absorption spectra of BDO based compounds **1**−**4** and BDT based compounds **5**−**7** is the relative intensity of the lower and higher wavelength peaks. In the absorption spectra of compound **1**−**4** both peaks have almost similar intensity, whereas the higher wavelength absorption peaks for compound **5**−**7** have significantly lower intensity than that of lower wavelength absorption peaks. Thus the absorption intensity of the low-energy band decreases in intensity upon moving from BDO-

based compounds to BDT-based compounds. This can be ascribed to the decreasing electronegativity of the heteroatom (from oxygen to sulfur). As the electronegativity of the oxygen is higher, the BDO unit has higher ability to produce and stabilize a charge-separated state.[12,42] The gaps between the highest occupied molecular orbital (HOMO) and lowest unoccupied molecular orbital (LUMO) of **1**−**7** were calculated 2.30−2.47 eV from onset absorption wavelength values, which, are comparable to those obtained from DFT calculations at B3LYP/6-31G(d). The absorption peaks of all the compounds in the solid state (Figure 1b) were red shifted compared to their solution spectra which indicated considerable intermolecular interaction in the solid state.

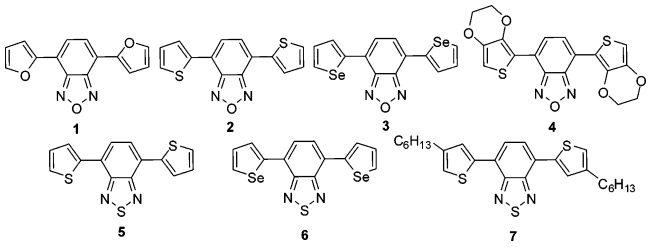


The electrochemical properties of **1**−**4**[41] and **5**−**7** were studied in acetonitrile, and tetrabutylammonium perchlorate (TBAPC) was used as supporting electrolyte (Supporting Information, Figure S1). The HOMO energy levels of **1**−**7** were calculated from onset values of the first oxidation potentials by using the equation HOMO = $-(E_{ox} - 0.35 + 4.81)$ eV, where the onset oxidation potential of Fc relative to the Ag/AgCl reference electrode is 0.35 V. The HOMO levels of **1**−**7** were in the range of −5.37 to −5.70 eV corresponding to the onsets of their first oxidation potentials of 0.91 to 1.24 V. The EDOT-based compound **4** showed the lowest oxidation potential among the four BDO-based compounds because of the presence of the more electron-rich moiety EDOT. Benzooxadiazole based compounds **2** and **3** showed slightly higher values for first oxidation potentials than that of their benzothiadiazole (BDT) analogues **5** and **6**. The difference between the first oxidation potential of **2** and **3** was greater than that of between **5** and **6**. It can be attributed to the greater electron acceptance property of BDO which makes it more difficult to extract an electron from the D−A−D systems. In other words the better electron accepting property of BDO stabilizes the HOMO levels in compounds **1**−**4**.

**Single Crystal X-ray Analysis.** Crystals of compounds **2**, **3**, **5**, and **6** were obtained by slow evaporation method from hexane/ethyl acetate. Crystallographic data and structure refinement parameters are listed in Table 2. The torsion angles between aromatic heterol rings and the central BDO/ BDT (C3, C4, C5, and C10; C12, C11, C8, and C9) in **2** (−8.1 and −170.2°), **3** (−1.0 and −177.9°), **5** (−178.5 and −4.7°), and **6** (−176.0 and −176.8°) indicate a nearly planar structure for all four compounds (Figure 2). Significant $\pi$-stacking (except for the compound **6**) and considerable short contacts have been observed in their crystal packing. In the crystal structures of compounds **2**, **3**, and **5** five membered aromatic heterocycles (thiophene and selenophene) are arranged anti to each other, whereas in the crystal structure of compound **6** two selenophene rings are syn to each other. It may be attributed strong Se···N intramolecular interaction in **6** (Se···N distance is

**Table 2. Crystallographic Data and Structure Refinement Parameters**

| | $C_{14}H_8N_2OSe_2$ | $C_{14}H_8N_2OS_2$ | $C_{14}H_8N_2SSe_2$ | $C_{14}H_8N_2S_3$ |
|---|---|---|---|---|
| crystal system | orthorhombic | orthorhombic | orthorhombic | orthorhombic |
| space group | *Pna*2(1) | *Pbca* | *Pca*2(1) | *Pbca* |
| $a$ [Å] | 19.874(5) | 10.049(5) | 16.1045(14) | 12.807(2) |
| $b$ [Å] | 5.1023(12) | 19.090(11) | 12.8052(10) | 9.9871(18) |
| $c$ [Å] | 12.693(3) | 12.528(7) | 6.4559(5) | 20.311(3) |
| $\alpha$ [deg] | 90 | 90 | 90 | 90 |
| $\beta$ [deg] | 90 | 90 | 90 | 90 |
| $\gamma$ [deg] | 90 | 90 | 90 | 90 |
| $V$ [Å$^3$] | 1287.0(6) | 2403(2) | 1331.34(19) | 2597.8(8) |
| $Z$ | 4 | 8 | 4 | 8 |
| $\lambda$ [Å] | 0.71073 | 0.71073 | 0.71073 | 0.71073 |
| $\rho_{calcd}$ [g cm$^{-3}$] | 1.962 | 1.572 | 1.967 | 1.536 |
| $F$[000] | 728.0 | 1168 | 760 | 1232 |
| $\mu$ [mm$^{-1}$] | 5.736 | 0.433 | 5.696 | 0.555 |
| $\theta$ [deg] | 2.05−23.61 | 2.68−25.11 | 2.53−25.58 | 2.77−23.72 |
| index ranges | $-22 \le h \le 22$ | $-8 \le h \le 12$ | $-19 \le h \le 19$ | $-14 \le h \le 14$ |
| | $-5 \le k \le 3$ | $-23 \le k \le 23$ | $-15 \le k \le 14$ | $-11 \le k \le 7$ |
| | $-14 \le l \le 14$ | $-15 \le l \le 15$ | $-7 \le l \le 7$ | $-16 \le l \le 23$ |
| $T$ [K] | 100(2) | 100(2) | 100 (2) | 100 (2) |
| $R1$ | 0.0505 | 0.1505 | 0.0427 | 0.0581 |
| $wR2$ | 0.1274 | 0.3799 | 0.1146 | 0.1545 |
| $R_{merge}$ | 0.0790 | 0.2026 | 0.0577 | 0.0955 |
| parameters | 155 | 137 | 172 | 172 |
| GOF | 1.077 | 1.587 | 0.942 | 1.075 |
| reflns total | 8477 | 18790 | 22474 | 9954 |
| unique reflns | 1906 | 2318 | 2239 | 2074 |
| obsd reflns | 1390 | 1464 | 1862 | 1342 |
| CCDC No. | 933354 | 933355 | 933356 | 933357 |

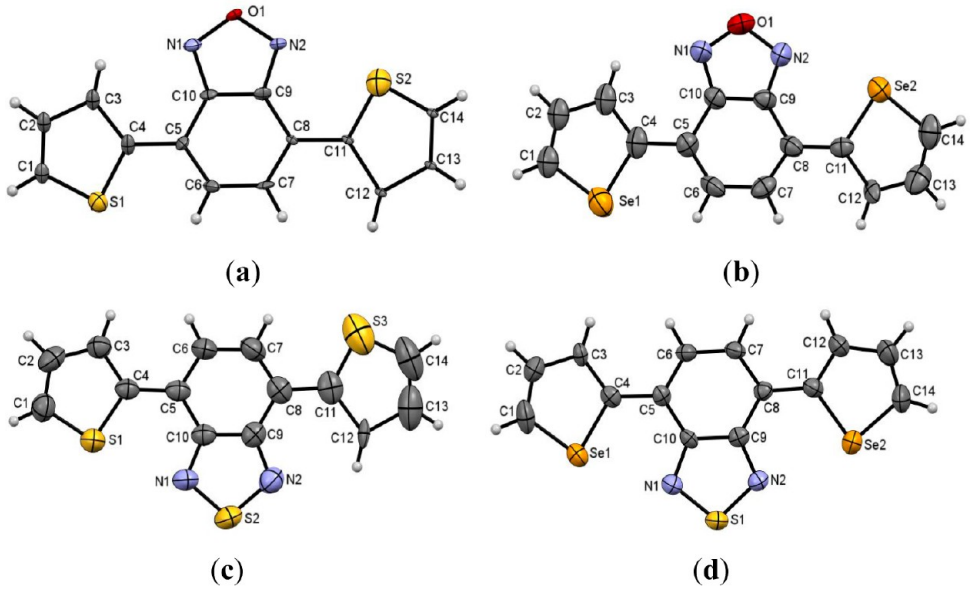


**Figure 2.** ORTEP representation of (a) **2**, (b) **3**, (c) **5**, and (d) **6** (Thermal ellipsoids are drawn at 50% probability level).

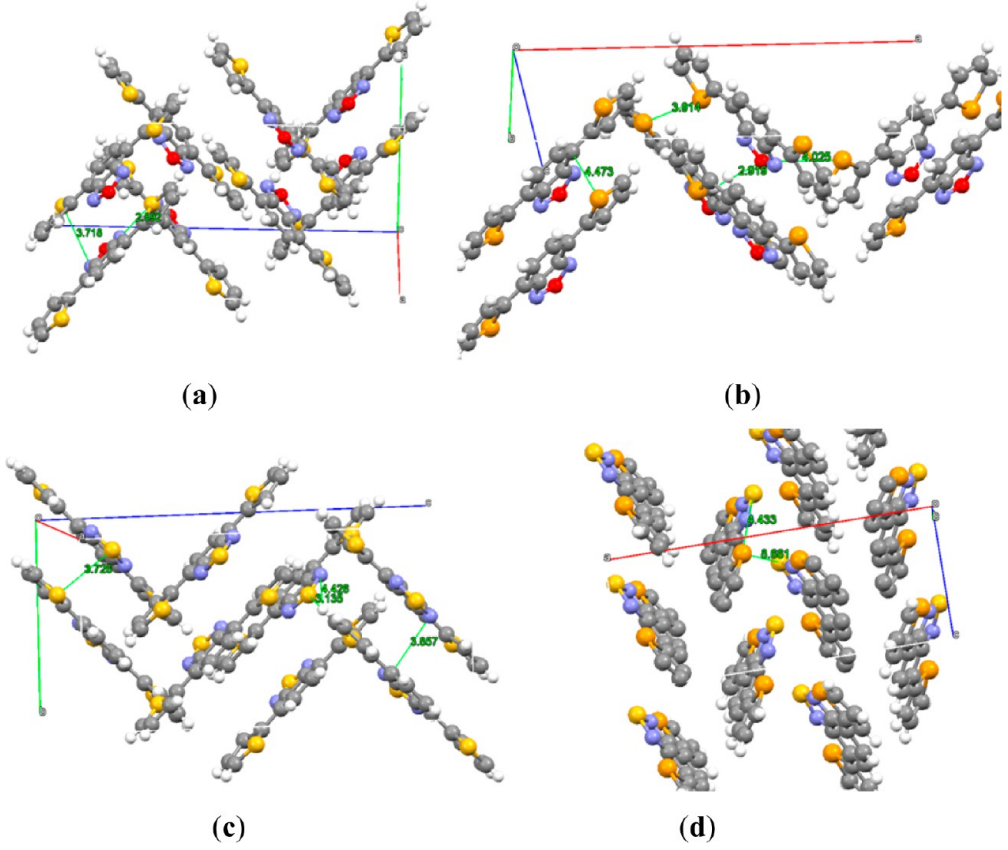


**Figure 3.** Crystal packing structure of (a) **2**, (b) **3**, (c) **5**, and (d) **6**.

2.88 Å). It results in the significantly different packing pattern of crystal structure of **6** compared with that of compounds **2**, **3**, and **5**.

Crystal packing of compounds **2**, **3**, **5**, and **6** are shown in Figure 3. The molecular packing in the crystal structures of **2**, **3**, and **5** follows a similar pattern. Considerable $\pi$-stacking interactions between the donor of one molecule and the acceptor of another molecule form an infinite ribbon type network which would facilitate efficient charge hopping. The molecules in the crystal structure of **2** and **5** array in such a way that benzochalcogenadiazole rings of adjacent molecules participating in $\pi$-stacking interactions are arranged anti to each other; whereas in case of **3** these are disposed in syn fashion. In compounds **2**, **3**, and **5** the distances between the two adjacent molecular planes are 3.43, 3.50, and 3.52 Å, respectively (Supporting Information, Figure S2). Additionally,

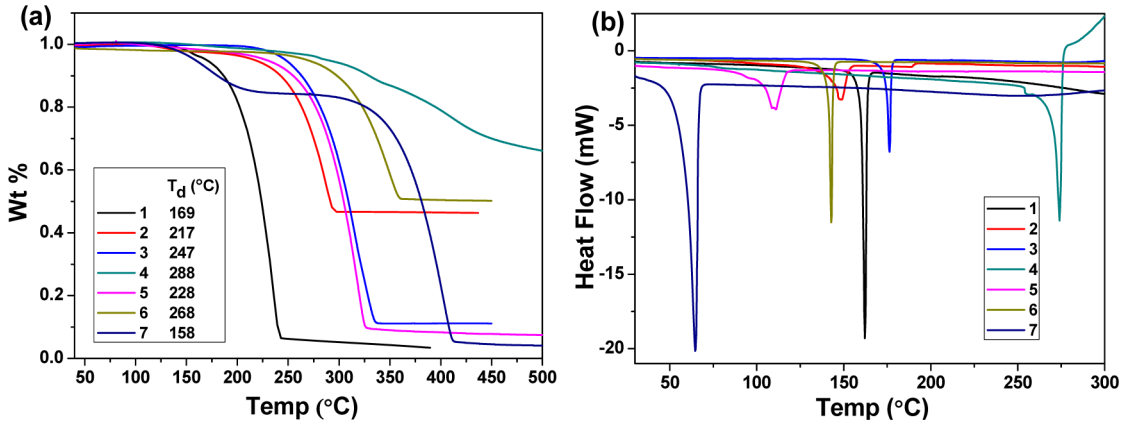


**Figure 4.** (a) TGA and (b) DSC thermogram of compounds **1**–**7** recorded under nitrogen atmosphere with a scan rate 10 °C/min.

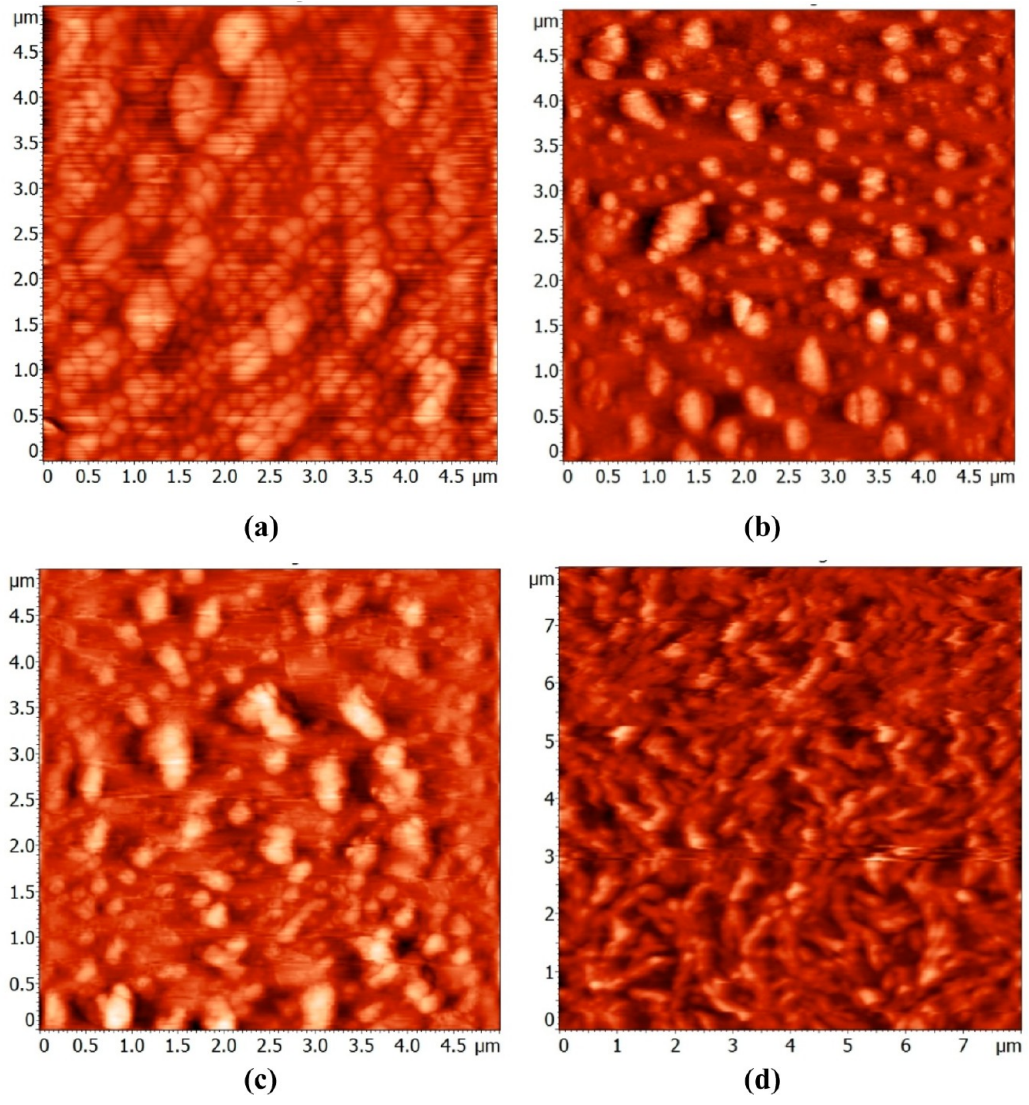


**Figure 5.** Surface morphology of (a) **2**, (b) **3**, (c) **5**, and (d) **6** films deposited onto $Si/SiO_2$ at rt.

crystal packing of **2** has N···H (2.584 Å), O···H (2.662 Å), S···H (2.933 Å), S···O (3.264 Å), and CH···$\pi$ (2.739, 2.813 Å) intermolecular interactions which lead to a 2D-interlock type of packing. The Se···H (3.067 Å) and CH···$\pi$ (2.832 Å) intermolecular interactions led the structure of **3** into 2D-interlock type of packing. Crystal packing of compound **5** exhibited N···H (2.749 Å) and CH···$\pi$ (2.870 Å) intermolecular interactions forming 2D-interlock type of packing. Compound **6** showed a different packing pattern than that for **2**, **3**, and **5**. Crystal packing of **6** does not possess any $\pi$–$\pi$ interactions. Compound **6** shows a herringbone packing pattern with S···$\pi$ (3.412, 3.492 Å), Se···$\pi$ (3.434, 3.563 Å), CH···$\pi$ (2.841, 2.883

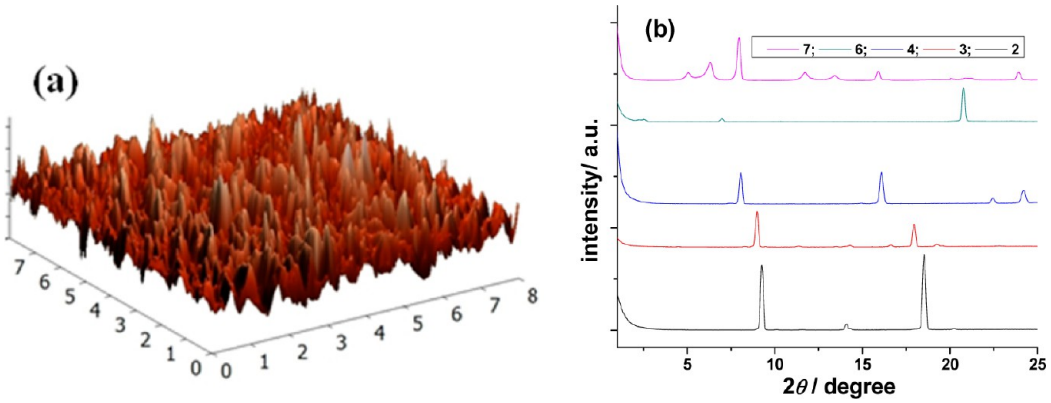


**Figure 6.** (a) Surface morphology in 3D films of **6** deposited onto $Si/SiO_2$ at rt; (b) XRD patterns of the compounds **2**−**4**, **6**, and **7** as-cast film at rt.

Å), and Se···S (3.560 Å) intermolecular interaction. Thus the combination of chalcogen atoms of benzochalcogenadiazole and chalcogenophene in D-A-D molecules has great impact on their molecular packing in crystal structures. The difference in the crystal packing (slipped stack structures or herringbone packing based on the disposition of the chalcogenophene rings around benzochalcogenadiazole) is interesting in view of crystal engineering of D-A-D structures.

**Theoretical Calculations.** In the crystal structure of compound **6** selenophene rings are arranged in syn fashion with selenium pointing towards the thiadiazole ring in contrast to the molecular structure of **2**, **3**, and **5** where chalcogenophenes are arranged in anti fashion to each other. To get more insight, DFT calculations were carried out at the B3LYP/6-31G(d) level. Compounds **2**, **3**, **5**, and **6** were optimized in both forms; that is, with syn and anti arrangement of hetereols to each other. (Supporting Information, Table S2). The syn form of **6** is more stable by 0.9 kcal/mol than its anti form, whereas anti forms of **2**, **3**, and **5** are stabler than their syn forms by 1.5, 0.2, 0.7 kcal/mol. It can be explained by stabilization of the structure of **6** in syn form by a two Se···N non-bonding interaction. Mulliken charge distribution in compounds **3** and **6** at the B3LYP/6-31G(d) level showed more negative charge on nitrogen in compound **6** (−0.596) than that in the compound **3** (−0.266), whereas selenium has nearly the same charge in both compounds (0.138 and 0.129 in **3** and **6**, respectively). In compound **3**, N atoms are covalently bonded with more the electronegative oxygen atom compared to sulphur in **6**. Therefore, availability of N-lone pair in **3** for Se···N nonbonding interaction is significantly decreased than in **6**. For compound **4** the syn-form is more stable than the anti-form because of the sustitution effect (ethylenedioxy substitution).

**Thermal Behavior.** Thermal stability of compounds **1**−**7** was examined by therogravimetric analysis (TGA) (Figure 4a). Compounds **1**−**7** exhibited their decomposition temperature ($T_d$) in the range of 158−288 °C. Furan derivative **1** decomposes after its melting point and thiophene and selenophene derivatives **2**, **3**, **5**, and **6** decompose in the range of 220−270° C indicating comparable stability. However, EDOT decomposes relatively at higher temperature because of the close packing structure. Selenophene containing compounds **3** and **6** have higher melting points than the corresponding thiophene derivatives **2** and **5**. The differential scanning calorimetry (DSC) analysis displayed only one sharp and strong endothermic peak with high enthalpy for all seven compounds related to their melting points (Figure 4b). All the compounds melted in the region 110−140° C except compounds **4** and **7**. Compound **7** showed very low melting point, which can be attributed to two hexyl chains on thiophenes. The high melting point of **4** indicated the closed packing structure for **4** with two EDOT moieties.

**Thin Film Morphologies.** The morphologies of compounds in thin film were investigated by atomic force microscopy (AFM) and powder X-ray diffraction (p-XRD). For p-XRD study films were prepared on glass slides from the chlorobenzene solution at room temperature by the spin coating method whereas for AFM study films were deposited on a $Si/SiO_2$ plate. AFM images of compounds **2**, **3**, **5**, and **6** indicate good film forming property of the compounds with rms surface roughness ~4.65 nm (Figure 5). Films of **2**, **3**, and **5** have shown the formation of larger grains. Compound **6** showed formation of continuous film in contrast to the films of **2**, **3**, and **5** (Figure 6a). p-XRD measurements on the thin films of **2**, **3**, and **5** showed sharp peaks at $2\theta$ in the region of 7.5°−9.0°, which correspond to the d-spacing of 10−12 Å (Figure 6b, Supporting Information, Table S2). The molecular lengths of all the molecules obtained from the single crystal X-ray analysis are in the range of 12−13 Å. It indicates the slanted orientation of molecules on the substrate. This observation matches with single crystal structure analysis. Compound **6** showed a different d-spacing in the p-XRD pattern. As a result, compound **6** has a herringbone type of packing, and compounds **2**, **3**, and **5** have interlock type packing. Additionally one strong peak toward wider angles with d spacing of 4.18−5.56 Å can be assigned to the cofacial interlayer $\pi-\pi$ stacking between the conjugated main chains.

**Field Effect Transistor.** Top contact bottom gate field effect transistors (FET) were fabricated for the transport studies of these compounds using procedures as described in reference 43. The compounds exhibited reasonably good p-type hole mobility ($\mu_{FET}$) (Figure 7) estimated from the saturation regime of operation. FETs were fabricated with different dielectrics, and semiconducting films were grown both by spin-coating and solution shearing method to optimize the device performance. Devices fabricated (5−10 in each case) from these compounds showed well-defined linear and saturation behavior with current modulation in the range of $10^3$ to $10^4$ (Table 3). Typical $\mu_{FET}$ values were in the range of 0.01−0.08 $cm^2\ V^{-1}\ s^{-1}$ for FETs fabricated with semiconducting films grown by solution shearing. The higher magnitude of $\mu_{FET}$ in these compounds compared with that of other related compounds[33,34,36,44−46] can be directly correlated to the strong inter-molecular interactions due to formation of D-A-D

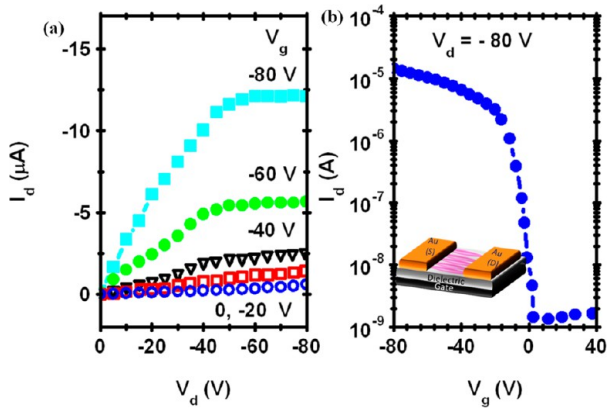


**Figure 7.** (a) Output and (b) transconductance curves for compound **6** with transistor prepared by solution sheared semiconducting film. Dimensions of the device are $W \approx 1$ mm and $L \approx 60$ $\mu$m, and BCB is the dielectric layer having $C_i \sim 4$ nF/cm$^2$. Inset (top) shows the schematic of the device. Similar characteristics were obtained for other molecules.

**Table 3. FET Transport Parameters for Different Molecules under Varied Fabrication Conditions**

| compound | dielectric | coating method | $\mu_{FET}^{max}$ ($cm^2 V^{-1} s^{-1}$) | $\mu_{FET}^{avg}$ ($cm^2 V^{-1} s^{-1}$) | $I_{on}/I_{off}$ |
|---|---|---|---|---|---|
| **1** | BCB | spin | 0.0516 | 0.0244 | $> 10^4$ |
| **2** | HFP | spin | 0.0035 | 0.0028 | $> 10^3$ |
| | | shear | 0.0084 | 0.0054 | |
| **3** | HFP | spin | 0.0042 | 0.003 | $> 10^4$ |
| | | shear | 0.01 | 0.008 | |
| **4** | BCB | spin | 0.0475 | 0.0185 | $> 10^3$ |
| **5** | BCB | spin | 0.06 | 0.038 | $> 10^4$ |
| | | shear | 0.04 | 0.015 | |
| **6** | BCB | spin | 0.0425 | 0.025 | $> 10^3$ |
| | | shear | 0.077 | 0.04 | |
| **7** | BCB | spin | 0.0351 | 0.0126 | $> 10^4$ |

structures and co-planarity of the molecule. Charge transport in conjugated molecules is governed by the transfer integral between the neighboring molecules ($t_{direct}$). In the case of these D-A-D structures with a slipped stack geometry, direct overlap between the neighboring donor molecules is reasonable. However, enhanced charge transport observed can be explained by the super-exchange nature of the electronic coupling. Charge coupling can occur between the orbitals of donor molecules with the orbitals of the bridging acceptor molecules. This super-exchange transfer integral ($t_{eff}$) can be larger than $t_{direct}$ in the presence of appropriate intermolecular stacking.[47] Additionally, these molecules form a highly planar crystalline structure and aggregates because of strong intermolecular interaction which makes the transport more tolerant to disorder or defects. High mobility of these compounds can be possibly attributed to the combination of these parameters. Contact resistance ($R_c$) does not play a significant role because of the relatively long channel length of the devices used ($L = 60-120$ $\mu$m). The transmission line method is utilized to estimate the $R_c$ for a FET with Au source-drain electrode. $R_c$ was obtained to be in the range of (43−68) KΩ while the channel resistance was of the order of 10 MΩ indicating the negligible effect of $R_c$. However, devices fabricated with Al as S-D electrode for one of the molecules demonstrated injection-limited linear response indicative of high $R_c$. Conductivity ($\sigma$) of the molecules was obtained to be in the range of 0.05−0.1 S cm$^{-1}$. The trends in $\sigma$ for different molecules were similar to the trends observed with $\mu_{FET}$. It is interesting to understand the origin of high $\mu_{FET}$ values for these small conjugated molecules.[48−50] The origin of enhanced transport properties of these molecules compared to other conjugated small molecules can be traced to the combination of microscopic and macroscopic properties obtained from efficient crystal and molecular engineering. From classical Marcus theory, the ease for charge transport in conjugated small molecules is governed by the transfer integral between the neighboring molecules and the re-organization energy involved during the transport process. In case of these D-A-D molecules the crystal structure shows a 2D slipped stack arrangement and an extremely co-planar structure with a torsional angle in the range of 2°−5°. The DFT calculated HOMO and LUMO of molecules **2**, **3**, **5**, and **6** are depicted in the Supporting Information, Figure S4. Electron density in the HOMO is delocalized throughout the entire conjugated backbone; however, in the LUMO the electron density is localized over the acceptor unit (BDO or DBT). Both these conditions favor efficient overlap between the orbitals to obtain enhanced $\pi-\pi$ stacking. Single crystal packing indicates the distance between two consecutive molecules to be in the range of 3.4−3.5 Å. Additionally, the transport pathway in these compounds is mainly governed by the conjugated backbone, so a planar backbone with a 2D packing will result in a relatively defect free transport. High mobility of these compounds can be possibly attributed to the combination of parameters originating from crystalline order, stronger intermolecular interaction, and molecular co-planarity. To further understand the role of defects originating from the interface, FETs were also fabricated with different dielectric layer like PVDF-HFP (dielectric constant = 8). FETs fabricated with this polar dielectric demonstrate much lower magnitude of $\mu_{FET}$. This can be directly related to the dipolar induced disorder originating from a polar environment at the interface which causes broadening of the Gaussian density of states (DOS). Hence, the observed low magnitude of $\mu_{FET}$ for molecules **2** and **3** is due to the trap induced disorder at the interface which can be a qualitative measure of the activation energy for transport.

Interestingly, the molecules **2**, **3**, and **6** had the propensity to form ordered crystallites (Supporting Information, Figure S5) when sheared during the drying process. This is reflected in the narrower and sharper XRD features of the films after shearing (Supporting Information, Figure S3). Increase in the sharpness and intensity of the peak can be attributed to increased crystallite size and decreased amorphous regions in the film. Apparently in these systems, the electrical transport parameters enhance with degree of order induced by shearing. Transport measurements were carried out for both parallel and perpendicular directions of the elongated crystallites. Significant anisotropy is obtained in the macroscopic transport property with the anisotropy ratio ($\mu_{FET}^{\parallel}/\mu_{FET}^{\perp}$) in the magnitude of 10−20, where $\mu_{FET}^{\parallel}$ is the mobility when the S-D electrodes are along the length of the crystallite and $\mu_{FET}^{\perp}$ is when the S-D electrodes are along the width of the crystallite. In general for these compounds $\mu_{FET}^{\parallel} > \mu_{FET}^{\perp}$, which can be attributed to the increase in the number of grain boundaries encountered by the charge carriers as they traverse along the width of the crystal compared with along the length of the crystallite.[51]

The variation of heteroatom in these compounds modifies the intermolecular interactions significantly which is reflected in the crystal structure and packing. However, OFETs fabricated

from compounds with a different heteroatom did not show significant variation in mobility. This possibly arises from the electronic structure of the transport band which primarily consists of contributions from the conjugated backbone of the molecule as opposed to the heteroatom. So heteroatoms attached to the core are not expected to contribute to transport because of the non-availability of density of states.[52]

## EXPERIMENTAL SECTION

To synthesize all the compounds one common high yielding procedure was used, that is, Stille coupling. Synthesis of compound **1**, **2**, **3**, and **4** were recently reported by our group.[41] Compounds **5**, **6**, and **7** were synthesized by following reported literature procedure.[53,54] Electrochemical studies were carried out with a Princeton Applied Research 263A potentiostat using platinum (Pt) disk electrode as the working electrode, a platinum wire as counter electrode, and an AgCl-coated Ag wire, which was directly dipped in the electrolyte solution, as the reference electrode. Nonaqueous Ag/AgCl wire was prepared by dipping silver wire in a solution of $FeCl_3$ and HCl. Pt disk electrodes were polished with alumina, water, and acetone and were dried with nitrogen gas before use to remove any incipient oxygen. The electrolyte used was 0.1 M TBAPC in ACN. UV−vis spectra were recorded on a HITACHI U-4100 UV−vis−NIR spectrophotometer. Crystal data was collected at room temperature (rt) on Bruker's KAPPA APEX II CCD Duo with graphite monochromated Mo−K$\alpha$ radiation (0.71073 Å). The intensity data were processed using Bruker's suite of data processing programs (SAINT), and absorption corrections were applied using SADABS.[55] Crystal structures were solved by direct methods using SHELXS-97, and the data was refined by full matrix least-squares refinement on $F^2$ with anisotropic displacement parameters for non-H atoms, using SHELXL-97.[56] Figures are drawn from X-seed version 2.0.[57]

**Device Fabrication.** Detailed transport study of these D-A-D molecules (**1**−**7**) was performed using bottom gate top contact FET geometry. Al metal is coated as the gate electrode by physical vapor deposition ($10^{-6}$ mbar, 40 nm thick) on pre-cleaned RCA treated glass substrate. Different dielectric layers were coated to optimize the formation of semiconducting film on the dielectric layer. The dielectric films used in the present study includes divinyltetramethylsiloxanebis-benzocyclobutene (BCB) and poly-vinylidene fluoride hexafloropropylene (PVDF-HFP). The dielectric films were coated by the procedure as reported elsewhere.[43] Capacitance properties of the dielectric layer were measured directly using the inbuilt C−V meter in a Keithley 4200 semiconductor parameter analyzer. Typical dielectric thickness is estimated to be around 0.4−0.5 $\mu$m as measured using Filmetrics (F20-EXR) thickness measurement set up. The capacitance values obtained were in the range of (4−15) nF/cm$^2$ for different dielectrics. The surface of all the dielectrics was coated (1500 rpm for 30 s) with a thin monolayer of hexamethyldisilazane (HMDS) and then annealed at 110°C for 2 h. The compound layer is then introduced from solution phase (25 mg/mL in chlorobenzene) by spin coating at 200 rpm for 1 minute to obtain films of thickness 50−80 nm. No annealing was performed on the optimized devices. Annealing the semiconducting films resulted in rupture and disruptions in the films. Mobility for the samples were obtained using the equation: $I_{ds} = (\mu_{FET}\, WC/2L)\,(V_g - V_{th})^2$ ,where $I_{ds}$ is the drain current,$W$ and $L$ are, respectively, the channel width and length, $C$ is the capacitance per unit area of the gate insulator layer, $V_{gs}$ and $V_{th}$ are the gate voltage and the threshold voltage respectively. Molecules **2**, **3**, and **6** formed crystals with solution shearing at the speed of 3 mm/s. Such solution sheared crystalline films demonstrated better $\mu_{FET}$. The choice of the S-D electrodes is decided from the HOMO levels obtained from the oxidation potential of the compound which closely matches gold electrodes for efficient injection. Devices were then completed by coating Au source-drain (S-D) electrodes at ($10^{-6}$ mbar, 40 nm thick). S-D electrodes were coated both along the alignment direction of the crystals and perpendicular to the crystals to observe the anisotropy in the transport.

## CONCLUSIONS

A series of D-A-D type molecules comprising benzooxadiazole (BDO) and benzothiadiazole (BDT) core symmetrically linked to two aromatic-heterols (furan (F), thiophene (T), and selenophene (Se)) at 4 and 7-positions has been studied for their physicochemical properties. Single crystal X-ray analyses of **2**, **3**, **5**, and **6** revealed that the combination of chalcogen atoms of benzochalcogenadiazole and chalcogenophene in D-A-D molecules has great impact on their molecular packing in crystal structures. The molecules **2**, **3**, **5**, and **6** are nearly planar with significant short range interactions such as $\pi\cdots\pi$, CH$\cdots\pi$, S$\cdots\pi$, Se$\cdots\pi$, N$\cdots$H, O$\cdots$H, S$\cdots$H, Se$\cdots$H, S$\cdots$O, and Se$\cdots$N interactions, which determine the crystal packing and orientation of the capped heterol ring with respect to central BDO or BDT unit. Strong intermolecular interactions arising from D-A-D structures along with significant planarity of these solution processable molecules may be responsible for high performance in FET devices. Compounds **2**, **3**, and **6** have the propensity to form ordered crystallites when sheared during the drying process in the thin films. These molecules pave the way for obtaining high performance small molecules by intelligent crystal engineering and molecular design. Strong intermolecular interactions arising from D-A-D structures along with significant planarity of these solution processable molecules is responsible for the high performance in FET devices. The technique of shearing is also used to form ordered crystallites which further enhances the field effect transport.

## ASSOCIATED CONTENT

### Supporting Information

Cyclic voltammetry of **5**, **6**, and **7**; figure including anisotropic crystal growth upon shearing; change in p-XRD pattern upon shearing; HOMO-LUMO pictures of **2**, **3**, **5**, and **6**; details of the theoretical calculation and coordinates of the optimized geometry. This material is available free of charge via the Internet at http://pubs.acs.org.

## AUTHOR INFORMATION

### Corresponding Authors

*E-mail: narayan@jncasr.ac.in (K.S.N.).
*E-mail: sanjiozade@iiserkol.ac.in (S.S.Z.).

### Notes

The authors declare no competing financial interest.

## ACKNOWLEDGMENTS

P.B.P. and S.P.S. thank UGC-India and CSIR-India, respectively, for their fellowship. S.S.Z is thankful to DRDO-India for funding.

## REFERENCES

(1) Newman, C. R.; Frisbie, C. D.; da Silva, D. A. F.; Bredas, J. L.; Ewbank, P. C.; Mann, K. R. *Chem. Mater.* **2004**, *16*, 4436−4451.
(2) Sirringhaus, H. *Adv. Mater.* **2005**, *17*, 2411−2425.
(3) Gershenson, M. E.; Podzorov, V.; Morpurgo, A. F. *Rev. Mod. Phys.* **2006**, *78*, 973−989.
(4) Menard, E.; Meitl, M. A.; Sun, Y. G.; Park, J. U.; Shir, D. J. L.; Nam, Y. S.; Jeon, S.; Rogers, J. A. *Chem. Rev.* **2007**, *107*, 1117−1160.
(5) Murphy, A. R.; Frechet, J. M. J. *Chem. Rev.* **2007**, *107*, 1066−1096.
(6) Azarova, N. A.; Owen, J. W.; McLellan, C. A.; Grimminger, M. A.; Chapman, E. K.; Anthony, J. E.; Jurchescu, O. D. *Org. Electron.* **2010**, *11*, 1960−1965.

(7) de Gans, B. J.; Duineveld, P. C.; Schubert, U. S. *Adv. Mater.* **2004**, *16*, 203−213.
(8) Koren, A. B.; Curtis, M. D.; Francis, A. H.; Kampf, J. W. *J. Am. Chem. Soc.* **2003**, *125*, 5040−5050.
(9) Chung, D. S.; Kong, H.; Yun, W. M.; Cha, H.; Shim, H.-K.; Kim, Y.-H.; Park, C. E. *Org. Electron.* **2010**, *11*, 899−904.
(10) Das, S.; Zade, S. S. *Chem. Commun.* **2010**, *46*, 1168−1170.
(11) Haid, S.; Mishra, A.; Uhrich, C.; Pfeiffer, M.; Bauerle, P. *Chem. Mater.* **2011**, *23*, 4435−4444.
(12) Das, S.; Pati, P. B.; Zade, S. S. *Macromolecules* **2012**, *45*, 5410−5417.
(13) Gidron, O.; Dadvand, A.; Sheynin, Y.; Bendikov, M.; Perepichka, D. F. *Chem. Commun.* **2011**, *47*, 1976−1985.
(14) Gandini, A. *Macromolecules* **2008**, *41*, 9491−9504.
(15) Binder, J. B.; Ronald, R. T. *J. Am. Chem. Soc.* **2009**, *131*, 1979−1985.
(16) Anthopoulos, T. D.; Anyfantis, G. C.; Papavassiliou, G. C.; de Leeuw, D. M. *Appl. Phys. Lett.* **2007**, *90*, 122105−122107.
(17) Usta, H.; Risko, C.; Wang, Z. M.; Huang, H.; Deliomeroglu, M. K.; Zhukhovitskiy, A.; Facchetti, A.; Marks, T. J. *J. Am. Chem. Soc.* **2009**, *131*, 5586−5608.
(18) Wang, S.; Gao, P.; Liebewirth, I.; Kirchhoff, K.; Pang, S.; Feng, X.; Pisula, W.; Mullen, K. *Chem. Mater.* **2011**, *23*, 4960−4964.
(19) Miyata, Y.; Yoshikawa, E.; Minari, T.; Tsukagoshi, K.; Yamaguchie, S. *J. Mater. Chem.* **2012**, *22*, 7715−7717.
(20) Qiu, L.; Yu, C.; Zhao, N.; Chen, W.; Guo, Y.; Wan, X.; Yang, R.; Liu, Y. *Chem. Commun.* **2012**, *48*, 12225−12227.
(21) Pho, T. V.; Yuen, J. D.; Kurzman, J. A.; Smith, B. G.; Miao, M.; Walker, W. T.; Seshadri, R.; Wudl, F. *J. Am. Chem. Soc.* **2012**, *134*, 18185−18188.
(22) Zhang, M.; Tsao, H. N.; Pisula, W.; Yang, C.; Mishra, A. K.; Mullen, K. *J. Am. Chem. Soc.* **2007**, *129*, 3472−3473.
(23) Lee, J.-K.; Gwinner, M. C.; Berger, R.; Newby, C.; Zentel, R.; Friend, R. H.; Sirringhaus, H.; Ober, C. K. *J. Am. Chem. Soc.* **2011**, *133*, 9949−9951.
(24) Lin, Y.; Fan, H.; Li, Y.; Zhan, X. *Adv. Mater.* **2012**, *24*, 3087−3106.
(25) Dhanabalan, A.; Duren, J. K. J.; Hal, P. A.; Dongen, J. L. J.; Janssen, R. A. J. *Adv. Funct. Mater.* **2001**, *11*, 255−262.
(26) Horie, M.; Kettle, J.; Yu, C.-Y.; Majewski, L. A.; Chang, S.-W.; Kirkpatrick, J.; Tuladhar, S. M.; Nelson, J.; Saunders, B. R.; Turner, M. L. *J. Mater. Chem.* **2012**, *22*, 381−389.
(27) Distler, A.; Kutka, P.; Sauermann, T.; Egelhaaf, H.-J.; Guldi, D. M.; Nuzzo, D. D.; Meskers, S. C.; Janssen, R. A. J. *Chem. Mater.* **2012**, *24*, 4397−4405.
(28) Padhy, H.; Huang, J.-H.; Sahu, D.; Patra, D.; Kekuda, D.; Chu, C.-W.; Lin, H.-C. *J. Polym. Sci., Part A: Polym. Chem.* **2010**, *48*, 4823−4834.
(29) Cheng, X.; Noh, Y.-Y.; Wang, J.; Tello, M.; Frisch, J.; Blum, R.-P.; Vollmer, A.; Rabe, J. P.; Koch, N.; Sirringhaus, H. *Adv. Funct. Mater.* **2009**, *19*, 2407−2415.
(30) Kono, T.; Kumaki, D.; Nishida, J.; Sakanoue, T.; Kakita, M.; Tada, H.; Tokito, S.; Yamashita, Y. *Chem. Mater.* **2007**, *19*, 1218−1220.
(31) Marrocchi, A.; Seri, M.; Kim, C.; Facchetti, A.; Taticchi, A.; Marks, T. J. *Chem. Mater.* **2009**, *21*, 2592−2594.
(32) Kono, T.; Kumaki, D.; Nishida, J.; Tokito, S.; Yamashita, Y. *Chem. Commun.* **2010**, *46*, 3265−3267.
(33) Melucci, M.; Favaretto, L.; Zanelli, A.; Cavallini, M.; Bongini, A.; Maccagnani, P.; Ostoja, P.; Derue, G.; Lazzaroni, R.; Barbarella, G. *Adv. Funct. Mater.* **2010**, *20*, 445−452.
(34) Crivillers, N.; Favaretto, L.; Zanelli, A.; Manet, I.; Treier, M.; Morandi, V.; Gazzano, M.; Samor, P.; Melucci, M. *Chem. Commun.* **2012**, *48*, 12162−12164.
(35) Black, H. T.; Dadvand, A.; Liu, S.; Ashby, V. S.; Perepichka, D. F. *J. Mater. Chem. C* **2013**, *1*, 260−267.
(36) Caputo, B. J. A.; Welch, G. C.; Kamkar, D. A.; Henson, Z. B.; Nguyen, T.-Q.; Bazan, G. C. *Small* **2011**, *7*, 1422−1426.
(37) Jiang, J.-M.; Yang, P.-A.; Chen, H.-C.; Wei, K.-H. *Chem. Commun.* **2011**, *47*, 8877−8879.
(38) Ding, P.; Zhong, C.; Zou, Y.; Pan, C.; Wu, H.; Cao, Y. *J. Phys. Chem. C* **2011**, *115*, 16211−16219.
(39) Blouin, N.; Michaud, A.; Gendron, D.; Wakim, S.; Blair, E.; Plesu, R. N.; Durocher, G.; Tao, Y.; Leclerc, M. *J. Am. Chem. Soc.* **2008**, *130*, 732−742.
(40) Ozkut, M. I.; Algi, M. P.; Oztas, Z.; Algi, F.; Onal, A. M.; Cihaner, A. *Macromolecules* **2012**, *45*, 729−734.
(41) Pati, P. B.; Das, S.; Zade, S. S. *J. Polym. Sci., Part A: Polym. Chem.* **2012**, *50*, 3996−4003.
(42) Gibson, G. L.; McCormick, T. M.; Seferos, D. S. *J. Am. Chem. Soc.* **2012**, *134*, 539−547.
(43) Senanayak, S. P.; Guha, S.; Narayan, K. S. *Phys. Rev. B* **2012**, *85*, 115311−115319.
(44) Ando, S.; Nishida, J.-I.; Inoue, Y.; Tokito, S.; Yamashita, Y. *J. Mater. Chem.* **2004**, *14*, 1787−1790.
(45) Nishinaga, T.; Miyata, T.; Tateno, M.; Koizumi, M.; Takase, M.; Iyoda, M.; Kobayashi, N.; Kunugi, Y. *J. Mater. Chem.* **2011**, *21*, 14959−14966.
(46) Romanazzi, G.; Aquila, A. D.; Suranna, G. P.; Marinelli, F.; Cotrone, S.; Altamura, D.; Giannini, C.; Torsi, L.; Mastrorilli, P. *J. Mater. Chem.* **2011**, *21*, 15186−15189.
(47) Zhu, L.; Yi, Y.; Li, Y.; Kim, E. G.; Coropceanu, V.; Bredas, J. L. *J. Am. Chem. Soc.* **2012**, *134*, 2340−2347.
(48) Mushrush, M.; Facchetti, A.; Lefenfeld, M.; Katz, H. E.; Marks, T. J. *J. Am. Chem. Soc.* **2003**, *125*, 9414−9423.
(49) Miyata, Y.; Terayama, M.; Minari, T.; Nishinaga, T.; Nemoto, T.; Isoda, S.; Komatsu, K. *Chem.—Asian J.* **2007**, *2*, 1492−1504.
(50) Zhang, S.; Guo, Y.; Xi, H.; Di, C..; Yu, J.; Zheng, K.; Liu, R.; Zhan, R. X.; Liu, Y. *Thin Solid Films* **2009**, *517*, 2968−2973.
(51) Kabra, D.; Narayan, K. S. *Adv. Mater.* **2007**, *19*, 1465−1470.
(52) Heeney, M.; Zhang, W.; Crouch, D. J.; Chabinyc, M. L.; Gordeyev, S.; Hamilton, R.; Higgins, S. J.; McCulloch, I.; Skabara, P. J.; Sparrowe, D.; Tierney, S. *Chem. Commun.* **2007**, 5061−5063.
(53) Tang, Z.; Lei, T.; Jiang, K.; Song, Y.; Pei, J. *Chem.—Asian J.* **2010**, *5*, 1911−1917.
(54) Yang, R.; Tian, R.; Yan, J.; Zhang, Y.; Yang, J.; Hou, Q.; Yang, W.; Zhang, C.; Cao, Y. *Macromolecules* **2005**, *38*, 244−253.
(55) *SADABS* V2008-1; Bruker AXS: Madison, WI, 2008.
(56) Sheldrick, G. M. *SHELX 97, Program for Crystal Structure Determination*; University of Göttingen: Göttingen, Germany, 1997.
(57) Barbour, L. J. *X-Seed, Graphical Interface to SHELX-97 and POV-Ray*; University of Missouri; Columbia: Columbia, MO, 1999.